Journal of Energy Chemistry 37 (2019) 197–203

Contents lists available at ScienceDirect

Journal of Energy Chemistry

journal homepage: www.elsevier.com/locate/jechem

http://www.journals.elsevier.com/journal-of-energy-chemistry/

# Porous LiF layer fabricated by a facile chemical method toward dendrite-free lithium metal anode

Yanxia Yuan[a], Feng Wu[a,b], Guanghai Chen[a], Ying Bai[a,*], Chuan Wu[a,b,*]

[a] Beijing Key Laboratory of Environmental Science and Engineering, School of Materials Science & Engineering, Beijing Institute of Technology, Beijing 100081, China

[b] Collaborative Innovation Center of Electric Vehicles in Beijing, Beijing 100081, China

ARTICLE INFO

*Article history:*
Received 20 February 2019
Revised 19 March 2019
Accepted 20 March 2019
Available online 26 March 2019

*Keywords:*
Lithium metal anode
Porous LiF layer
Lithium dendrite
Artificial SEI

ABSTRACT

Lithium metal is supposed to be critical material for constructing next-generation batteries due to extremely high capacity and ultralow redox potential. However, the perplexing issue of lithium dendrite growth impedes the commercial application. The initial nucleation and low Li ions diffusion rate in the electrolyte/electrode interface dominate the deposition behavior. Therefore, a uniform and flexible interface is urgently needed. Here, a facile method is proposed to prepare a thin and porous LiF-rich layer (TPL) by the in-situ reaction of small amount of ammonium hydrogen difluoride ($NH_4HF_2$) and Li metal. The deposition morphology on Li metal anode with LiF layer is significantly flat and homogeneous owning to low lateral diffusion barrier on LiF crystals and the porous structure of TPL film. Additionally, the symmetrical cells made with such TPL Li anodes show significantly stable cycling over 100 cycles at high current density of 6 mA/cm$^2$. The TPL Li | $LiFePO_4$ full cells keep over 99% capacity retention after 100 cycles at 2.0 C. This approach serves as a facile and controllable way of adjusting the protective layer on Li metal.



## 1. Introduction

The demands for excellent consumer electronics, unmanned aerial vehicles and transport plane advocate innovations and breakthroughs in rechargeable battery technologies [1–4]. Now lithium ion batteries (LIBs) with the specific energies as high as 250 Wh/kg are available. For further improvement of energy density, the traditional anode materials, such as carbon materials, are unable to meet this demand [5]. Lithium metal possesses the highest theoretical capacity (3860 mAh/g) and the lowest potential (−3.040 V versus standard hydrogen electrode), which is considered as reserve force for the advanced energy storage system [6–8]. Although lithium metal was studied by numerous researches in the early time of LIBs, scientists had to move away the focus from lithium metal with daunting safety issues to graphite anodes with commercial success. Recent years, advanced experimental technologies and viewpoint have encouraged scientists to revisit this problem with neoteric notion and enhanced methods. As a result, the batteries made with lithium metal anode have a rapid development in the past few years [9].

Even great advances have been made with tremendous efforts, the instable interphase between the lithium metal electrode and liquid electrolyte gives rise to uneven Li deposition, which results in daunting lithium dendrite growth [10–12]. The sharp tree-like dendrite can penetrate the separator, inducing short circuit and explosion of rechargeable batteries. In addition, due to the uneven distribution of chemical components on lithium surface, the inhomogeneous plating/stripping of Li forms dendritic Li, which is fragile and easy to break off from the original conductive Li bulk, then results in “dead Li” and low Coulombic efficiency (CE). Meanwhile, the repeated damaging/rebuilding of solid electrolyte interphase (SEI) throughout the whole cycling brings about thick SEI growth and rapidly capacity fading. Hence, effective solutions should be developed to overcome these issues and prolong the lifetime of lithium metal batteries (LMBs) [13].

During past few years, plenty of efforts devoted to work out the issues and the challenges to enhance the safety and cycling performance of batteries [14,15], mainly bent on the optimization of electrolyte [16–20], the fabrication of multifunctional separators [21,22], the modification of anode and SEI film [23–26]. The properties of SEI film play pivotal role in affecting the depositional

* Corresponding authors at: Beijing Key Laboratory of Environmental Science and Engineering, School of Materials Science & Engineering, Beijing Institute of Technology, Beijing 100081, China.

*E-mail addresses:* membrane@bit.edu.cn (Y. Bai), chuanwu@bit.edu.cn (C. Wu).

https://doi.org/10.1016/j.jechem.2019.03.014
2095-4956/

behavior of Li ions [27]. Thus, previous works proposed numerous novel strategies to protect the lithium metal by the fabrication of robust artificial SEI film, including adding effective liquid electrolyte additives (FEC [18], VC [28], $CsPF_6$ [29,30], LiPS [31,32], $LiNO_3$ [33,34]) to build SEI film in-situ. Moreover, the utilization of emerging composite lithium salts, solvent or high concentrated electrolyte can increase the availability of Li ion concentration, as well as build a steady SEI film [35,36]. But the additives and lithium salts are constantly consumed, the structure or composition of SEI suffers from inevitably evolution. Thus, researchers developed ex situ artificial SEI by chemical or physical methods.

LiF has been considered as an effective protective layer due to the low energy barrier ($E_b$ = 0.19 eV in vacuum) for the diffusion of lithium ions and a high surface energy compared with other common SEI compounds [37]. In a previous work, a simple method prepared by in-situ reaction between $NH_4HF_2$ powder and bare lithium metal was proposed to build an artificial LiF-rich host on lithium metal surface [38]. The deposition morphology on the surface of Li metal anode with uniformly distributed porous LiF host is significantly flat. However, compared with other similar reports, the thickness of this artificial film is far greater than expected, though it works with excellent performance. Besides, the optimized thicknesses of the artificial protective layer, which is rich in LiF are not the same, ranging from nanoscale to micron-sized in previous studies. As reported by Liu et al., amount of Li (N/P ratio) is a key parameter for high-energy-density practical LMBs and additional improvement in specific energy can be achieved by significantly reducing the amount of Li. Thus, it is necessary to modify Li foil with ultrathin protective layer [39]. It is meaningful to further explore the performance of the same manufacturing method by applying it under extreme condition.

Indeed, the thickness of the artificial protective layer has an influence on the performance of LMBs. A recent work reported by Zhang's group indicated that the immersed lithium metal anode, which possesses thicker artificial layer, owns larger resistance and larger hysteresis voltage than that obtained by dropping small amount of precursor solution [40]. In this work, to obtain a thin and porous LiF-rich layer (TPL) with small interface impedance, we propose a facile method by dropping the weakly acidic $NH_4HF_2$-treatment solution on Li metal surface, different from our previous method that immersing Li foil into precursor solution for 24 h. To control the degree of reaction and obtain TPL film, air-laid paper is used to drain the excess liquid immediately after one drop of solution is spread evenly on Li metal surface. The as-obtained TPL film simultaneously possesses porous structure for lithium storage and presents high surface energy to prevent dendrite growth as previous work reported [38]. Moreover, the decreased thickness of LiF reduces the interface impedance significantly. These features of TPL film enable small polarization at high current density of 6 mA/cm$^2$. The Li | LFP full cell with TPL film on Li anode also exhibits stable cycling at the rate of 2 C, while the cells with bare Li decrease rapidly.

## 2. Experimental

### 2.1. Synthesis

All the chemicals were used without any purification. Lithium foils (China Energy Lithium Co. LTD, the thicknesses of Li foils are all 1 mm) were utilized as electrodes in two-electrode cells and full cells. Bare lithium foil was scrubbed by a scraper blade before further treatment. 0.08 g ammonium fluorine hydride ($NH_4HF_2$, from Alfa Aesar) powder was dissolved in 10 g dimethyl sulfoxide (DMSO, from Alfa Aesar) solution to acquire the precursor solution. Then the precursor solution was dropped on the surface of polished lithium foil by distribution droplets method. Excess solution was cleaned by lint-free wipe immediately. Then, the treated lithium foil was dried at room temperature in vacuum. The as-prepared lithium foil was denoted as TPL Li. The cathodes for full cells were fabricated by mixing $LiFePO_4$ powder, acetylene black as conductive additive, and polyvinylidene fluoride (PVDF) as binder with a weight ratio of 80:10:10. After processing, the cathode laminate was dried in a vacuum oven at 80 °C for 24 h. The loading of active material is about 3 mg/cm$^2$.

### 2.2. Electrochemical test

The electrolyte of Li|$LiFePO_4$ full cells was comprised of ethyl carbonate (EC)/diethyl carbonate (DEC) (1:1 in volume) with 1 M $LiPF_6$ powder dissolved. The electrolyte of two electrodes cells was comprised of 1,3-dioxolane (DOL)/1,2-dimethoxyethane (DME) (1:1 in volume) as solvent, and 1 M lithium bis(trifluoromethanesulfonyl) imide (LiTFSI) and 1 wt% $LiNO_3$ as solute. The Celgard 2400 separator was put between two electrodes. Coin cells CR2025 were assembled in an Ar-filled glove box (MBraun Labmaster130). The amount of electrolyte was limited to 60 µL in each cell.

### 2.3. Characterization

The cells (both before cycling and after cycling) were disassembled to get the anode samples. After washed in DME for three times and dried in air warehouse for 6 h, the anode samples were transferred into a sealed container for characterizations. Scanning electron microscopy (FE-SEM, HITACHI S-4800), X-ray diffraction (XRD, Rigaku Ultima IV-185 with Cu $K_\alpha$ radiation at a scan rate of $2\theta$ = 8 °/min), and X-ray photoelectron spectroscopy (XPS, PHI QUANTERA-II SXM system) were utilized to obtain surface morphology and analyze the surface composition. Energy-dispersive X-ray detector (EDX) tested the element analysis; A Land battery test system (CT2001A) was utilized to evaluate electrochemical performance of electrodes. Electrochemical impedance spectroscopy (EIS) was performance over a frequency from 1 × 105 Hz to 0.01 Hz with an AC perturbation signal of 5 mV and recorded on a CHI 660C electrochemical workstation.

## 3. Results and discussion

The LiF is widely accepted as a dominated chemical component in SEI film to enhance the depositional behavior due to the high Li ions diffusion rate and low energy barrier for Li ions transportation [37]. Thus, to build LiF layer on Li anode surface, a replacement reaction between Li metal and $NH_4HF_2$ ($NH_4HF_2 + Li \rightarrow LiF + NH_4F + H_2$) is occurred by direct contact between $NH_4HF_2$-containing solution and bare Li. The possibility of this reaction at room temperature is fully verified as shown in Fig. 1(a).

Compared with the modified Li metal obtained by dropping small amount of precursor solution, the immersed sample owns larger resistance and larger hysteresis voltage [40]. Therefore, we put forward a facile distribution droplets method to reduce the dosage of solution and reaction time to obtain a TPL film. The as-obtained TPL anode is covered by cuboid LiF particles uniformly (Fig. 2a). The diameters of LiF particles range from 22 nm to 52.4 nm. As shown in Fig. 2(b), the LiF particles are covered with fluoride element homogenously. As desired, the thickness of LiF layer is decreased to 6.86 µm. Compared with the mosaic structure of components distribution in routine SEI film [41]. The TPL film provides a phase-uniform and simple surface on Li anode.

The compositions of the TPL film are further analyzed by X-ray diffraction (XRD) and X-ray photoelectron spectroscopy (XPS) (Fig. 3). The XRD peaks at $2\theta$ = 36.9° and 65.3° are indexed as

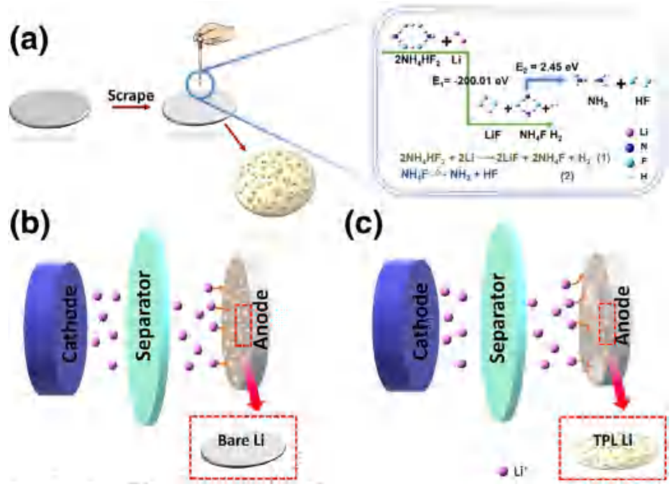


**Fig. 1.** (a) Schematic of the fabrication procedure of TPL Li. (b, c) The role of bare Li and TPL Li on the electrochemical reactions during plating.

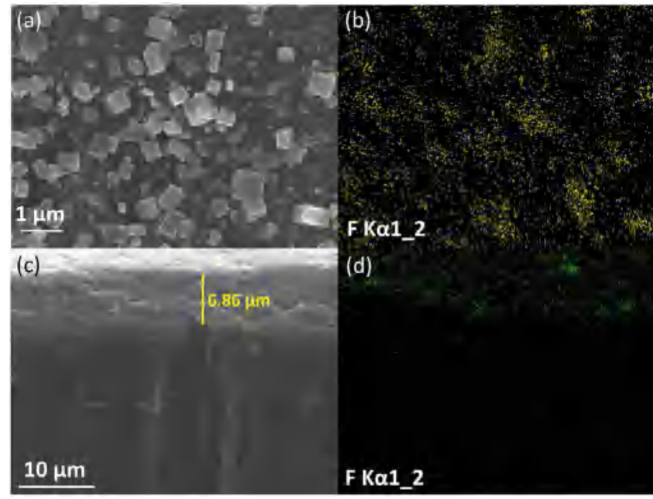


**Fig. 2.** The SEM images of the protective LiF layer on TPL Li. (a) The surface and (c) cross-section morphology of TPL Li anode. (b, d) The correlating element mapping of F.

LiF, which demonstrating the crystalline nature of the LiF particles (Fig. 3d). Auger electron spectroscopy is employed to characterize the chemical compositions of TPL film without the contamination of air on Li metal during data acquisition as shown in Fig. 3. With sputter depth profiling, the contents of Li and F tend to remain stable and become basis of the TPL film (inset in Fig. 3a), which suggesting that the LiF was formed uniformly and confirming that the replacement reaction occurs on the lithium metal surface, which are in accordance with previous report.

The interface stability of TPL anode is evaluated in the symmetrical cells at different current densities with a fixed capacity of 1 mAh/cm$^2$. The cell made with TPL anode displays long cycling stability both at 2 mA/cm$^2$ and 5 mA/cm$^2$. Even at a high current density of 6 mA/cm$^2$, the cells made with TPL anodes remain stable cycling. However, the cell made with bare Li is easy to come to failure stemmed from unstable interface evolution. When the cells cycled at 2.0 mA/cm$^2$ (Fig. 4a), the hysteresis voltage of two kinds of cells is nearly equal (≈50 mV) at the several former cycles (0–10). In addition, the overpotential of TPL cells remain stable within 350 h, while it displays serious polarization and the polarization increases drastically in bare Li metal cells. When the current densities are 5 and 6 mA/cm$^2$ (Fig. 4b, c), the cells with TPL anode keep stable cycling over 100 cycles, which is in significant contrast with unsteady interface variation of bare Li anode. The inset pictures in Fig. 4 display the local voltage-time curves for better evaluation. The cells with TPL Li show more excellent performance during long term cycling, suggesting that the fast ions diffusion rate of LiF is dominant at high current densities. The rate capability of the electrode with TPL film is also studied by cycling a symmetric cell at several current densities with the same cycling capacity (1 mAh/cm$^2$) (Fig. 5a). The cells with TPL have lower cell polarization than the cells with bare Li anode.

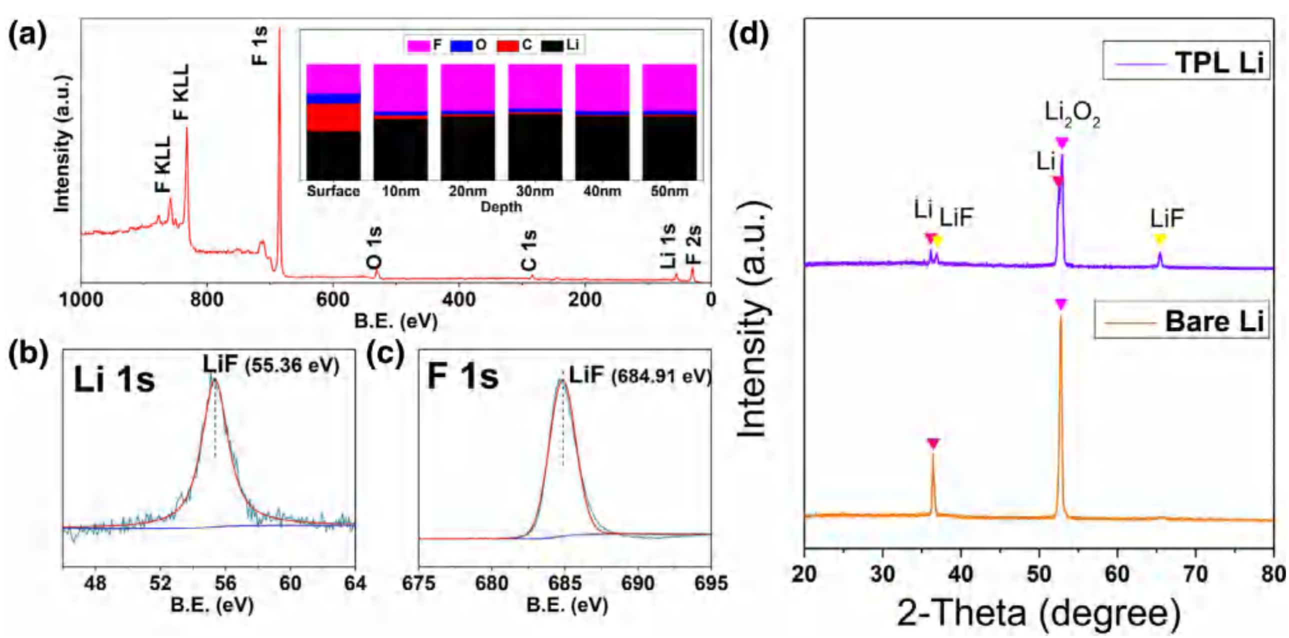


**Fig. 3.** Component characterizations of TPL Li. (a) X-ray photoelectron spectroscopy (XPS) of TPL film. (b) Li 1$s$ and (c) F 1$s$ spectra of TPL film. (d) XRD patterns of TPL Li and bare Li.

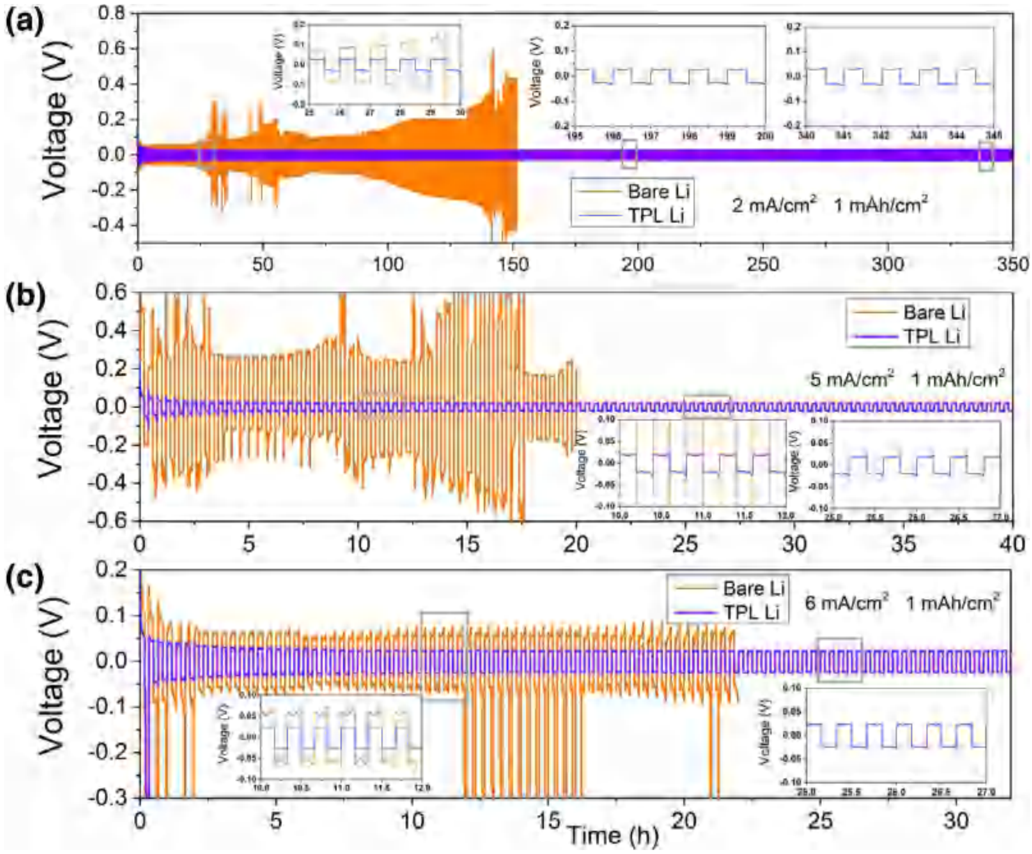


**Fig. 4.** Evaluation of lithium metal anode surface stability. Symmetrical cells with bare Li anode (orange) and TPL Li anode (purple) are cycling at (a) 2.0 mA/cm$^2$, (b) 5.0 mA/cm$^2$, and (c) 6.0 mA/cm$^2$, respectively (Electrolyte: 1 M LiTFSI in DME/DOL (1:1 in vol.) solvent and 1 wt% $LiNO_3$).

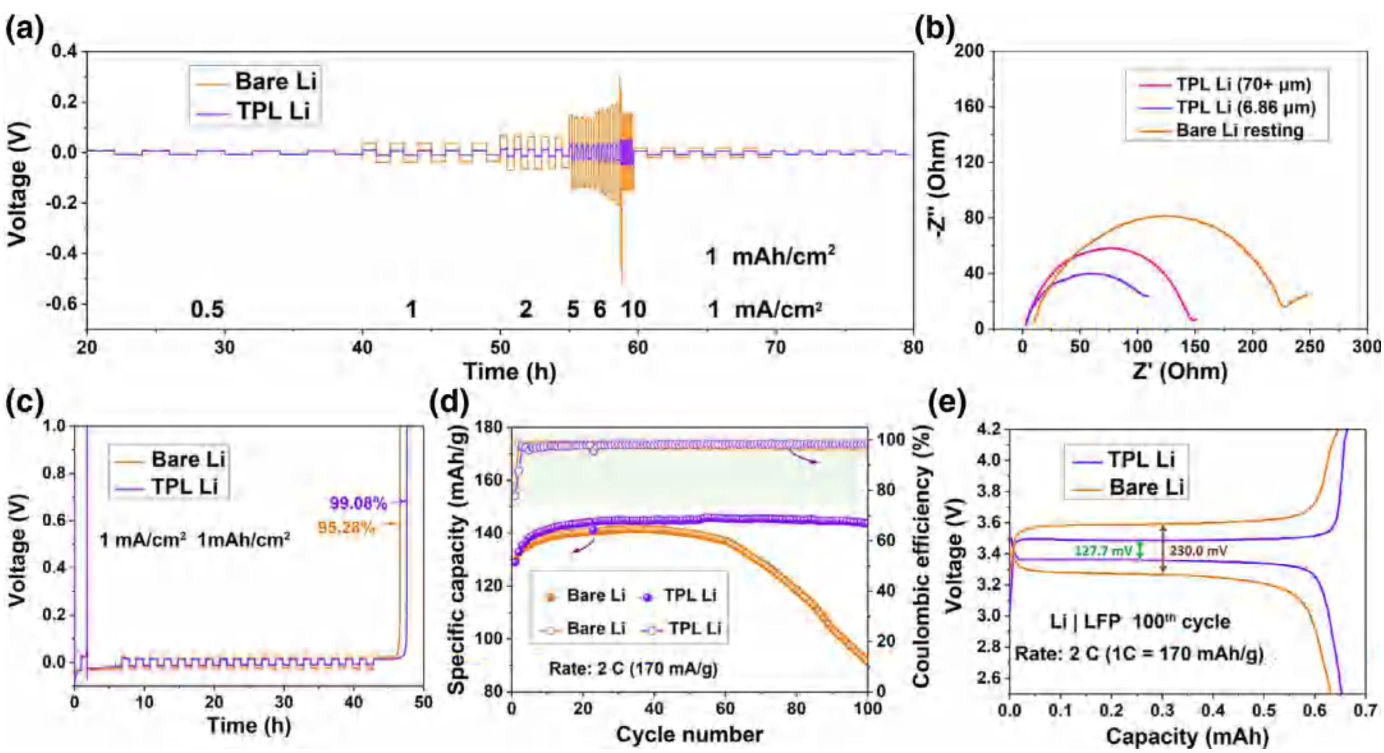


**Fig. 5.** (a) Rate capability of symmetrical cells with TPL Li and bare Li. (b) The interface impedance of symmetrical cells with different anodes before cycle. (c) The comparison of CE test. (d) Comparison of electrochemical performance of full cells with bare Li anode and TPL Li anode (rate = 2 C, 1 C = 170 mA/g). (e) Electrochemical curves of full cells with bare Li (orange) and TPL Li (purple) as anode, corresponding to the 100th cycle of (d).

The impedance of interface film has a significant effect on the cell polarization. To evaluate the influence of the thickness of LiF layer on the interface impedance, the electrochemical impedance spectroscopy (EIS) method was utilized to measure the interface resistance of both cells with bare Li and TPL Li, respectively (Fig. 5b). As revealed by EIS, the immersed Li anode (thickness = 70+ μm) owns larger resistance than TPL anode, and the interfacial resistance decreases with the reducing of the thickness (from 145 to 109 Ω). The decreased interface impedance is beneficial to enhance the electrochemical performance and reduce polarization that have been demonstrated in above-mentioned electrochemical performance.

As studied by Peled et al. [42,43] and Aurbach et al. [44,45], the SEI film has an significant influence on the cycling Coulombic efficiency (CE) of LMBs and has been studied extensively. The CE is usually decreased by the consumption of active materials caused by side reactions and dendrites growth on the Li surface. To obtain an accurate determination of CE, a rigorous method derived from Zhang's group is utilized to measure the TPL Li anode [46]. An initial formation process is wielding at 1 mA/cm$^2$ to relieve the initial loss affection, a fixed lithium layer (5.0 mAh/cm$^2$) is deposited on Li anode with/without TPL film by electrochemical control, and then the pre-deposited anode is utilized as the working electrode. After 20 cycles, the cell with TPL Li anode achieves a high CE of 99.08%, while the CE of cell with bare Li anode is just 95.28% (Fig. 5c). Through the analysis of aforementioned data between bare Li and TPL Li, LiF has significant effect on the interface stability of Li metal, which gives the credit to the improved Li ions diffusion rate and low energy barrier for Li ions transportation realized by LiF.

To investigate the practical application of TPL anode, $LiFePO_4$ cathode was utilized to pair TPL Li anode to assemble full cells. After several cycles of activation, the discharge capacity of the cell with TPL Li anode remains about 144 mAh/g, and still keep in 143.7 mAh/g after 100 cycles at 2.0 C (1.0 C = 170 mA/g). On the contrast, the discharge capacity of cells with bare Li anode remains stable cycling during the first 58 cycles, and displays a steep decrease in 59th cycle and decay to 91.3 mAh/g when the cells cycle to 100th cycle (Fig. 5d), which may be ascribed to the ceaseless consumption of active Li and electrolyte caused by the side reactions between bare lithium metal and liquid electrolyte. The excellent electrochemical performances in full cells indicate the stability of TPL film and its superiority in protecting the Li metal anode. Additionally, the CE of full cells with TPL Li remains above 98.2%, which is attributed to the existing of LiF layer protecting the Li metal from corrosion. As shown in Fig. 5(e), the Galvanostatical test curves reveal that the polarizing voltages of TPL film and routine SEI film are totally different when cycle number comes to 100 cycles. The polarization potential of cells with TPL anode is 127.7 mV, while that of cells with bare Li anode is 230 mV, which indicates that the cells with bare Li anode deteriorates quickly under high current densities due to the high polarizing potential. The porous LiF protective layer can effectively reduce side reaction under high current densities.

Since it has been demonstrated that the LiF-rich layer on Li metal anode can efficiently reduce production of Li dendrites because of the increased ions diffusivity and high surface energy. Thus, the characterization of surface evolution on bare Li and TPL Li after the first plating is also conducted which the current densities are 0.5 and 1.0 mA/cm$^2$ with the capacity of 1.0 and 2.0 mAh/cm$^2$. In contrast, the shape of deposited Li on TPL Li surface significantly differs from those on the bare Li. The morphology of deposited Li with two different plating capacities is shown in Fig. 6. During plating, Li ions initially pass through the LiF layer and finally deposit on the Li surface, with the plating progresses, the Li ions will deposit in the voids in the following stage and

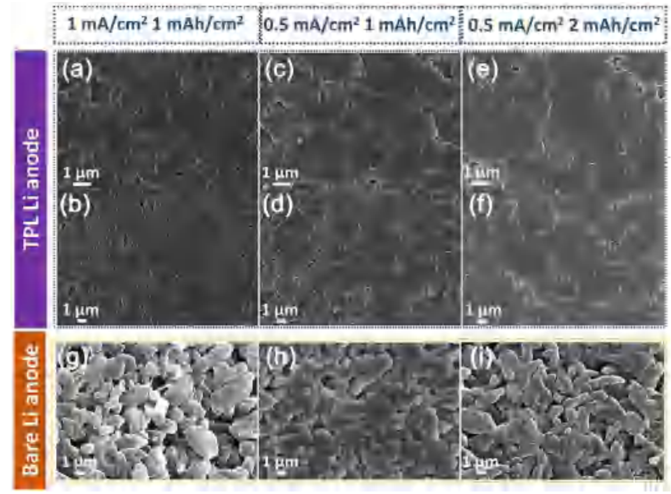


**Fig. 6.** The surface evolution of TPL Li (a–f) and bare Li (g–i) anodes after the initial deposition observed by SEM measurement. (a,b,g) Deposited at 1.0 mA/cm$^2$ (1.0 mAh/cm$^2$). (c,d,h) Deposited at 0.5 mA/cm$^2$ (1.0 mAh/cm$^2$). (e,f,i) Deposited at 0.5 mA/cm$^2$ (2.0 mAh/cm$^2$).

then covered on the LiF layer which results in dendrite-free morphology at last. As shown in Fig. 6(a–d), under the same cycling capacity, flatter Li deposition at the low current density is in corresponding to the Sand's time model. That is, low current density is benefit to ions' homogeneous diffusion and then restrain dendrite growth [47]. Under the same current density, the higher cycling capacity gives rise to the flatter Li deposition, which probably is attributed to the high quality deposition behavior during initial stage. However, under the same cycling conditions as TPL cells, the deposition morphology of bare Li anode surface is uneven and ramiform. Therefore, the TPL film is capable to restrain lithium dendrite growth efficiently, especially the porous structure of LiF layer can provide more space for Li deposition and LiF particles can guide the Li ions lateral and uniform diffusion.

The interface stability has a great effect on the long term cycling of LMBs. With the cells operating, the shape and components of interface change unceasing. Thus, to explore the surface evolution of TPL Li and bare Li anodes after long term plating/stripping cycles and provide more evidences to support the viewpoint mentioned before, SEM images are obtained to compare the surface morphology of those two kinds of anodes after 100 cycles (Fig. 7). It is shown that the existing of TPL film contributes to uniform and smooth Li deposition, while the bare Li surface is covered with uneven Li particles. Combined with the SEM images in Fig. 6, the dendrite-free morphology after the initial charging also demonstrate that LiF layer can accelerate the ions diffusion rate and benefit Li uniformly deposition. Under the same current density, higher cycling capacities are also characterized as shown in Fig. 8. With the capacity increases, the deposition morphology gets smoother and tends to deposit like scales. Even the capacity up to 10 mAh/cm$^2$, the cells with TPL Li anode can still run several cycles. The scaly deposition probably ensues from the high quality pre-deposition on TPL film.

A modified Li anode with thin and porous LiF film is fabricated. Based on aforementioned results, this TPL Li can effectively suppress Li dendrites and exhibits excellent stability and prolonged cycling life under high current density in symmetrical cell and Li|LFP full cell. Throughout these impressive results, this method has following traits: (1) Controllability of this facile method. Through adjust the dosage of precursor solution, the thinning of LiF layer enables low interfacial impedance and low polarization voltage at high current density. (2) Chemical stability of LiF during long term

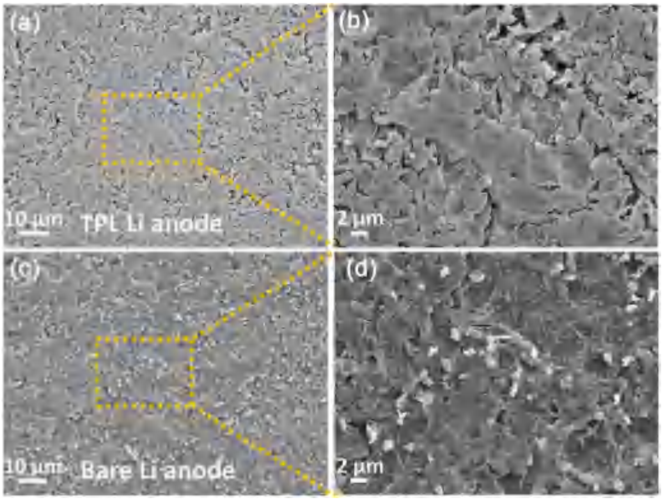


**Fig. 7.** The surface evolution of TPL Li (a, b) and bare Li (c, d) anodes after 100 cycles observed by SEM.

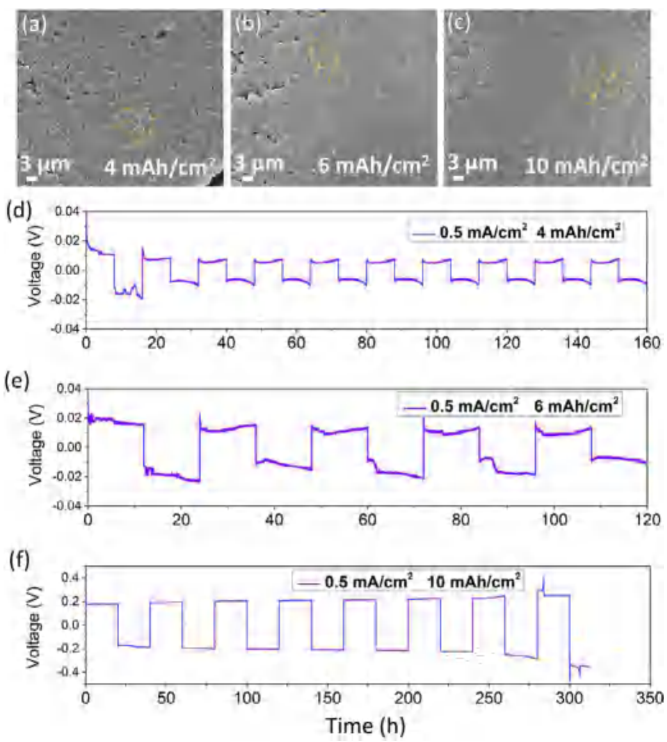


**Fig. 8.** Surface morphology observation of TPL Li anodes after initial deposition with cycling capacities of (a) 4.0 mAh/cm$^2$, (b) 6.0 mAh/cm$^2$, and (c) 10 mAh/cm$^2$. (d–f) The corresponding electrochemical performance of (a–c).

cycling. (3) Combine the benefits of LiF with porous structure to modify the Li metal surface. When nonuniform Li ions flux reaches the anode, it firstly passes through the LiF layer with high ions diffusion rate and then achieves homogenous distribution. Simultaneously, the porous structure provides more space for high capacity Li to deposit.

## 4. Conclusions

In conclusion, we propose a facile approach to fluoridate lithium metal surface by constructing a thin and porous LiF layer, which significantly decrease the interface impedance and reduce hysteresis voltage. Additionally, the as prepared LiF layer possesses following traits: (1) The thickness of LiF layer is greatly reduced and the porous structure in LiF layer is preserved. The voids existed in LiF layer provide Li deposition space, and then ensure the dendrite-free morphology even with high cycling capacity. (2) The LiF layer is chemically inert. It is beneficial to retard corrosion reactions between lithium metal and electrolyte. (3) The low energy barrier for Li ion transportation and high surface energy of LiF make for a flat and scale-like deposition morphology. And the dosage of precursor solution is greatly reduced, which is cost-effective. As thus, the symmetrical cells with TPL Li anode exhibit stable cycling at a high current density and prolonged cycling life at 2 mA/cm$^2$ (350 h, 1 mAh/cm$^2$). The capacity retention of TPL Li|LFP full cells is maintained over 99% after 100 cycles at 2.0 C. Therefore, this facile surface modification method provides an idea to fabricate thin and porous LiF layer on lithium metal. All these aforementioned features of this method make it a dependable option for the promoting of advanced LMBs.

## Acknowledgments

This work was supported by the National Basic Research Program of China (Grant no. 2015CB251100), and Beijing Natural Science Foundation (No. L182023).

## References

[1] E.C. Evarts, Nature 526 (2015) S93–S95.
[2] L. Grande, E. Paillard, J. Hassoun, J.B. Park, Y.J. Lee, Y.K. Sun, S. Passerini, B. Scrosati, Adv. Mater. 27 (2015) 784–800.
[3] C. Zhao, Y. Lu, J. Yue, D. Pan, Y. Qi, Y.S. Hu, L. Chen, J. Energy Chem. 27 (2018) 1584–1596.
[4] X. Zhang, Z. Zhang, Z. Zhou, J. Energy Chem. 27 (2018) 73–85.
[5] J. Janek, W.G. Zeier, Nat. Energy 1 (2016) 16141.
[6] X.B. Cheng, R. Zhang, C.Z. Zhao, Q. Zhang, Chem. Rev. 117 (2017) 10403–10473.
[7] F. Wu, Y.X. Yuan, X.B. Cheng, Y. Bai, Y. Li, C. Wu, Q. Zhang, Energy Storage Mater. 15 (2018) 148–170.
[8] X.B. Cheng, C. Yan, X.Q. Zhang, H. Liu, Q. Zhang, ACS Energy Lett. 3 (2018) 1564–1570.
[9] P.G. Bruce, S.A. Freunberger, L.J. Hardwick, J.M. Tarascon, Nat. Mater. 11 (2011) 19–29.
[10] X. Xu, S. Wang, H. Wang, C. Hu, Y. Jin, J. Liu, H. Yan, J. Energy Chem. 27 (2018) 513–527.
[11] L. Wang, Z. Zhou, X. Yan, F. Hou, L. Wen, W. Luo, J. Liang, S.X. Dou, Energy Storage Mater. 14 (2018) 22–48.
[12] K.N. Wood, E. Kazyak, A.F. Chadwick, K.H. Chen, J.G. Zhang, K. Thornton, N.P. Dasgupta, ACS Central Sci. 2 (2016) 790–801.
[13] R.V. Salvatierra, G.A. Lopez-Silva, A.S. Jalilov, J. Yoon, G. Wu, A.L. Tsai, J.M. Tour, Adv. Mater. 30 (2018) e1803869.
[14] L. Liu, C. Du, S. Wang, S. Chen, Chin. Chem. Lett. 29 (2018) 1781–1784.
[15] P. Zou, Y. Wang, S.W. Chiang, X. Wang, F. Kang, C. Yang, Nat. Commun. 9 (2018) 464.
[16] J. Zheng, M.H. Engelhard, D. Mei, S. Jiao, B.J. Polzin, J.G. Zhang, W. Xu, Nat. Energy. 2 (2017) 17012.
[17] C.Z. Zhao, X.Q. Zhang, X.B. Cheng, R. Zhang, R. Xu, P.Y. Chen, H.J. Peng, J.Q. Huang, Q. Zhang, Pro. Natl. Acad. Sci. 114 (2017) 11069–11074.
[18] X.Q. Zhang, X.B. Cheng, X. Chen, C. Yan, Q. Zhang, Adv. Funct. Mater. 27 (2017) 1605989.
[19] G. Zhang, H.J. Peng, C.Z. Zhao, X. Chen, L.D. Zhao, P. Li, J.Q. Huang, Q. Zhang, Angew Chem. Int. Ed. Engl. 57 (2018) 16732–16736.
[20] J. Cui, T.G. Zhan, K.D. Zhang, D. Chen, Chin. Chem. Lett. 28 (2017) 2171–2179.
[21] P.J. Kim, V.G. Pol, Adv. Energy Mater. 8 (2018) 1802665.
[22] D. Lin, D. Zhuo, Y. Liu, Y. Cui, J. Am. Chem. Soc. 138 (2016) 11044–11050.
[23] X.B. Cheng, C. Yan, H.J. Peng, J.Q. Huang, S.T. Yang, Q. Zhang, Energy Storage Mater. 10 (2018) 199–205.
[24] R. Xu, X.Q. Zhang, X.B. Cheng, H.J. Peng, C.Z. Zhao, C. Yan, J.Q. Huang, Adv. Funct. Mater. 28 (2018) 1705838.
[25] X. Shen, X. Cheng, P. Shi, J. Huang, X. Zhang, C. Yan, T. Li, Q. Zhang, J. Energy Chem. 37 (2019) 29–34.
[26] H. Dong, X. Xiao, C. Jin, X. Wang, P. Tang, C. Wang, Y. Yin, D. Wang, S. Yang, C. Wu, J. Power Sources 423 (2019) 72–79.
[27] X.B. Cheng, R. Zhang, C.Z. Zhao, F. Wei, J.G. Zhang, Q. Zhang, Adv. Sci. 3 (2016) 1500213.
[28] H. Ota, K. Shima, M. Ue, J.-i. Yamaki, Electrochim. Acta 49 (2004) 565–572.
[29] F. Ding, W. Xu, X. Chen, J. Zhang, Y. Shao, M.H. Engelhard, Y. Zhang, T.A. Blake, G.L. Graff, X. Liu, J.G. Zhang, J. Phy. Chem. C. 118 (2014) 4043–4049.

[30] Y. Zhang, J. Qian, W. Xu, S.M. Russell, X. Chen, E. Nasybulin, P. Bhattacharya, M.H. Engelhard, D. Mei, R. Cao, F. Ding, A.V. Cresce, K. Xu, J.G. Zhang, Nano Lett. 14 (2014) 6889–6896.
[31] C. Yan, X.B. Cheng, C.Z. Zhao, J.Q. Huang, S.T. Yang, Q. Zhang, J. Power Sources 327 (2016) 212–220.
[32] S. Xiong, K. Xie, Y. Diao, X. Hong, J. Power Sources 246 (2014) 840–845.
[33] Y. Liu, D. Lin, Y. Li, G. Chen, A. Pei, O. Nix, Y. Li, Y. Cui, Nat. Commun. 9 (2018) 3656.
[34] J. Guo, Z. Wen, M. Wu, J. Jin, Y. Liu, Electrochem. Commun. 51 (2015) 59–63.
[35] H. Dai, K. Xi, X. Liu, C. Lai, S. Zhang, J. Am. Chem. Soc. 140 (2018) 17515–17521.
[36] J. Qian, W.A. Henderson, W. Xu, P. Bhattacharya, M. Engelhard, O. Borodin, J.G. Zhang, Nat. Commun. 6 (2015) 6362.
[37] L. Fan, H.L. Zhuang, L. Gao, Y. Lu, L.A. Archer, J. Mater. Chem. A. 5 (2017) 3483–3492.
[38] Y. Yuan, F. Wu, Y. Bai, Y. Li, G. Chen, Z. Wang, C. Wu, Energy Storage Mater. 16 (2019) 411–418.
[39] J. Liu, Z. Bao, Y. Cui, E.J. Dufek, J.B. Goodenough, P. Khalifah, Q. Li, B.Y. Liaw, P. Liu, A. Manthiram, Y.S. Meng, V.R. Subramanian, M.F. Toney, V.V. Viswanathan, M.S. Whittingham, J. Xiao, W. Xu, J. Yang, X.Q. Yang, J.G. Zhang, Nat. Energy 4 (2019) 180–186.
[40] C. Yan, X.B. Cheng, Y.X. Yao, X. Shen, B.Q. Li, W.J. Li, R. Zhang, J.Q. Huang, H. Li, Q. Zhang, Adv Mater. 30 (2018) 1804461.
[41] N.W. Li, Y.X. Yin, C.P. Yang, Y.G. Guo, Adv. Mater. 28 (2016) 1853–1858.
[42] E. Peled, J. Electrochem. Soc. 126 (1979) 2047–2051.
[43] E. Peled, D. Golodnitsky, G. Ardel, J. Electrochem. Soc. 144 (1997) L208–L210.
[44] D. Aurbach, M.L. Daroux, P.W. Faguy, E. Yeager, J. Electrochem. Soc. 134 (1987) 1611–1620.
[45] D. Aurbach, Y. Ein-Ely, A. Zaban, J. Electrochem. Soc. 141 (1994) L1–L3.
[46] B.D. Adams, J. Zheng, X. Ren, W. Xu, J.G. Zhang, Adv. Energy Mater. 8 (2018) 1702097.
[47] W. Xu, J. Wang, F. Ding, X. Chen, E. Nasybulin, Y. Zhang, J.G. Zhang, Energy Environ. Sci. 7 (2014) 513–537.